**Astronomy & Astrophysics**

# Interstellar $^{12}$C/$^{13}$C from CH$^+$ absorption lines: results from an extended survey[*]

O. Stahl[1], S. Casassus[2], and T. Wilson[3,4]

[1] ZAH, Landessternwarte Königstuhl, 69117 Heidelberg, Germany
e-mail: O.Stahl@lsw.uni-heidelberg.de
[2] Departamento de Astronomía, Universidad de Chile, Casilla 36-D, Santiago, Chile
e-mail: simon@das.uchile.cl
[3] ESO, Karl-Schwarzschild-Str. 2, 85748 Garching bei München, Germany
e-mail: twilson@eso.org
[4] Max-Planck-Institut für Radioastronomie, Postfach 2024, 53010 Bonn, Germany

**ABSTRACT**

*Context.* The $^{12}$C/$^{13}$C isotope ratio in the interstellar medium (ISM) and its evolution with time are important tracers of stellar yields. Spatial variations in this ratio can be used to study mixing in the ISM.
*Aims.* We want to determine this ratio and its spatial variations in the local ISM from CH$^+$ absorption lines in the optical towards early-type stars. The aim is to determine the average value for the local ISM and to study possible spatial variations.
*Methods.* We observed a large number of early-type stars with Feros to extend the sample of suitable target stars for CH$^+$ isotope studies. The best-suited targets were observed with the Uves instrument with a higher signal-to-noise ratio and spectral resolution to determine the isotope ratio from the interstellar CH$^+$ lines. This study significantly expands the number of $^{13}$CH$^+$ detections.
*Results.* We find an average ratio of $\langle R \rangle = 76.27 \pm 1.94$ or, for $f = 1/R$, $\langle f \rangle = (120.46 \pm 3.02) \times 10^{-4}$. The scatter in $f$ is $6.3 \times \sigma(\langle f \rangle)$. This finding strengthens the case for chemical inhomogeneity in the local ISM, with important implications for the mixing in the ISM. Given the large scatter, the present-day value in the ISM is not significantly larger than the solar value, which is assumed to correspond to the local value 4.5 Gyr ago.

**Key words.** ISM: abundances – ISM: clouds – ISM: molecules – ISM: evolution – Galaxy: evolution – Galaxy: abundances

## 1. Introduction

The $^{12}$C/$^{13}$C ratio is a cornerstone of models of the nuclear history of our galactic interstellar matter (ISM), that is, the Galactic chemical evolution. Low and intermediate mass stars increase (during the AGB phase) the $^{12}$C/$^{13}$C ratio to ~300, while stars more massive stars (undergoing CNO processing) increase the ratio to $^{12}$C/$^{13}$C ~ 3. A measurement of the $^{12}$C/$^{13}$C ratio in the ISM thus provides important information about the relative importance of stars of different mass to the chemical enrichment of the interstellar matter.

The $^{12}$C/$^{13}$C ratio in the solar system is 89 (Anders & Grevesse 1989). Models of chemical evolution predict a decrease in the $^{12}$C/$^{13}$C ratio with time for a given galactocentric distance, and a decrease with galactocentric distance in the Galaxy (Prantzos et al. 1996). Such models assume that mixing in the ISM is complete and restricted to material at a given galactocentric distance (azimuthal mixing). A comparison of results between our Galaxy and other galaxies will give important data for the nuclear processing history (see, e.g., Tosi 2000; Prantzos 2001)

The $^{12}$C/$^{13}$C ratio has been determined mostly from radio-astronomical measurements of CO and H$_2$CO (see e.g., Wilson & Rood 1994) and millimeter observations of CN (Savage et al. 2002; Milam et al. 2005).

These results may be affected by interstellar chemistry in different ways, however: Chemical fractionation (which results from different zero-point energies of the isotopomers) enriches molecules in $^{13}$C (Watson et al. 1976) and thus lowers the ratio, selective dissociation destroys the rarer species more and thus raises the ratio. The latter effect is due to self-shielding of the more abundant isotopemer, which therefore survives photo-destruction better than the less abundant counterpart.

The molecule CH$^+$ is thought to be produced only in hotter parts of photo-dissociation regions and is a rare species, so is not affected by either chemical fractionation or selective dissociation. In addition, the optical CH$^+$ lines have typically only small saturation effects. This molecule, which can be observed in optical absorption lines from the ground, is therefore considered to provide the most secure $^{12}$C/$^{13}$C ratios (see e.g. Watson et al. 1976). We caution, however, that the formation process of CH$^+$ is probably not completely understood (Gredel et al. 1993).

Two systems of CH$^+$ lines are strong enough to be easily observed from the ground. In addition, the absorption lines from $^{12}$CH$^+$ at 4232 and 3957 Å are sufficiently shifted from their $^{13}$CH$^+$ component to allow unblended measurements,

---

provided the velocity profiles in the intervening cloud are narrow enough. If both are measured simultaneously, we can make use of the fact that the $^{13}$CH$^+$ line is blue-shifted by 0.26 Å relative to the $^{12}$CH$^+$ at 4232 Å but red-shifted by 0.44 Å relative to the $^{12}$CH$^+$ line at 3957 Å. This way, a chance superposition with another cloud along the line-of-sight can be excluded. In addition, the two simultaneous measurements help to eliminate systematic effects.

This property has been used e.g. by Stahl & Wilson (1992) to check that there is no accidental overlap of a weak velocity component of $^{12}$CH$^+$ at $-18.8$ km s$^{-1}$ from the deepest $^{12}$CH$^+$ absorption line with the $^{13}$CH$^+$ line. Nearly all previous data were taken at 4232 Å only.

These measurements in the optical require, however, observations with high spectral resolution and signal/noise ratio. Most of the published CH$^+$-measurements have therefore been obtained with very bright background stars at relatively small distances from the Sun.

The availability of efficient high-resolution spectrographs at 8 m-class telescopes in recent years has improved the situation considerably (Casassus et al. 2005, in the following Paper I). The observations are hampered, however, by the scarcity of suitable published candidate stars with sufficiently strong and narrow CH$^+$ absorption lines. In this paper we present new observations which have been obtained at targets specifically selected for this purpose.

The outline of the paper is as follows: Sect. 2 describes our observations. Section 3 gives details on our procedure to measure the isotopic ratio $R$. The results are discussed in Sect. 4, both the average properties of the sample and notes about individual targets. Section 5 discusses the results and concludes the paper.

## 2. Observations and reduction

### 2.1. Pre-selection with Feros

Many of the published CH$^+$-measurements are hampered either by too broad or complex line profiles of the interstellar lines. The isotope shift is very small, so that for most sight-lines (with relatively broad absorption lines) the isotopic lines partly overlap, which introduces considerable errors to the isotope ratio. Interstellar lines with several components are even more problematic. The best lines of sight have sharp, single absorption lines.

The stars with published CH$^+$-profiles that are suitable for the determination of the $^{12}$C/$^{13}$C isotope ratio are exhausted by previous studies. We therefore undertook a dedicated search for additional targets, which might be suitable for studies of the isotope ratio.

For this purpose we used the FEROS echelle spectrograph at the ESO/MPI 2.2 m telescope at ESO, La Silla. FEROS has a sufficiently high spectral resolution (48 000) to examine the CH$^+$ line profiles. In three nights in January 2006 we observed about 80 early-type stars with a B magnitude brighter than 8.0 selected from various lists (Humphreys 1978; Maíz-Apellániz et al. 2004).

The exposure times for the FEROS spectra were relatively short (typically a few minutes), just long enough to give a reasonable S/N-ratio near the $\lambda$4232, 3957 lines of CH$^+$. The $^{13}$CH$^+$ component is not detected in these spectra. The FEROS data were pipeline-reduced directly at the telescope. From these

spectra we selected the targets which were best suited for follow-up observations with UVES. The main selection criteria were:

– sharp and symmetric CH$^+$-lines;
– high equivalent width and;
– brightness of the target in the $B$ band.

The sharpest and deepest absorptions are needed to separate $^{13}$CH$^+\lambda$4232 from $^{12}$CH$^+\lambda$4232. We first selected by inspection the narrowest and single-component absorptions, with line profiles close to a single Gaussian. We then ordered individual lines of sight according to two quantitative indicators of sharpness. The first indicator is the signal-to-noise ratio on the absorption line, $\gamma = D/\sigma = W_\lambda \sqrt{F_c}/\Delta = W_\lambda 10^{-0.2B}/\Delta$, where $D$ is the depth of the line, $W_\lambda = (\sqrt{\pi}/(2\sqrt{2\ln 2}))D\Delta/F_c$ its equivalent width, and $\Delta$ its full width at half maximum, $\sigma \propto \sqrt{F_c}$ is the noise, and $B$ is the $B$-band magnitude of the background star. The second indicator, introduced to weight the final ranking towards the sharpest lines, was simply $\gamma_\Delta = \gamma/\Delta$. The final list of stars selected and later observed with UVES is given in Table 1.

Since the FEROS spectra cover a large spectral range (3600–9200 Å) we also obtained information about many other interstellar lines. A paper describing the full FEROS data set is in preparation.

### 2.2. High S/N observations with Uves

Observations of the selected stars with high S/N were obtained with the UVES echelle spectrograph at the VLT unit telescope Kueyen at Cerro Paranal, Chile, in three nights between January 8/9 and January 10/11, 2006. UVES allows measuring both line systems in the same detector setting, thus providing a means to correct for line blending if it is apparent in the spectra.

The observations are difficult because of the need for both very high S/N and very high spectral resolution to acquire the profile of faint $^{13}$CH$^+$, against a very bright stellar continuum and close to the much stronger $^{12}$CH$^+$ component. We need S/N ratios of at least ~10 on $^{13}$CH$^+$ for accurate profile fitting.

The project requires the highest possible spectral resolution. We therefore used an image slicer to minimize flux losses. In addition, the image slicer distributes the light along the slit, which improves flat-fielding and allows longer integration times before saturation occurs. UVES slicer #2 was used, which reformats an entrance opening of 1$''$8 × 2$''$2 to a slit of 0$''$44 width and a length of 7$''$9, which is imaged on the spectrograph entrance slit of 0$''$45 width. The spectral resolution in this configuration is $\lambda/\Delta\lambda = 75\,000$. The central wavelength was set to 4370 Å, which gives a spectral coverage from 3730 to 5000 Å. During our observations the seeing was sometimes too good to fill the entrance aperture of the images slicer. Therefore, for some spectra, only one or two slices contained most of the signal, which unfortunately decreases the gain of the image slicer.

Accurate flat-fielding is also important. Therefore a large number of flat-fields (150) was obtained during day-time distributed along the observing run.

In addition, two rapidly rotating unreddened early-type stars (HD 10144 = $\alpha$Eri, spectral type B3Ve and HD 108248 = $\alpha^1$Cru, spectral type B0.5IV) were observed in order to check for possible faint telluric features. These stars have been observed with exactly the same instrumental settings as the target stars and with similar S/N-ratio. We confirm there are no detectable telluric features under the CH$^+$ absorption.

The brighter targets where exposed until about 50% of the maximum level allowed by the CCD detector was reached. This

**Table 1.** Summary of the observations. The table columns contain the HD number, spectral type, $B$ magnitude, average airmass, total integrated exposure time and the number of exposures for each target.

| Target | Spec. | $B$ | Airmass | Exp. [s] | Number |
|--------|-------|-----|---------|----------|--------|
| HD 10144 | B3Ve | 0.3 | 1.36 | 63 | 90 |
| HD 23480 | B6IVe | 4.11 | 1.52 | 1100 | 55 |
| HD 35149 | B1V | 4.85 | 1.16 | 3920 | 98 |
| HD 37903 | B1.5V | 7.91 | 1.13 | 5760 | 24 |
| HD 52266 | O9V | 7.22 | 1.15 | 606 | 3 |
| HD 52382 | B1Ib | 6.64 | 1.05 | 4800 | 40 |
| HD 53974 | B0.5IV | 5.44 | 1.03 | 3020 | 60 |
| HD 58510 | B1Iab | 6.91 | 1.04 | 5000 | 25 |
| HD 73882 | O9III | 7.58 | 1.05 | 6257 | 27 |
| HD 75149 | B3Ia | 5.68 | 1.09 | 5400 | 90 |
| HD 76341 | B1/B2Ib | 7.39 | 1.06 | 6000 | 25 |
| HD 91452 | B0III | 7.66 | 1.30 | 5760 | 24 |
| HD 92964 | B2.5Iae | 5.59 | 1.22 | 3900 | 65 |
| HD 108248 | B0.5IV | 1.32 | 1.31 | 20 | 20 |

to typically a few minutes for our targets. Series of up to 50 exposures per target were obtained to build up the required S/N-ratio. Targets which turned out to show too complex line profiles were dropped from the target list. The observations are summarized in Table 1, which also lists the mean airmass of the target objects in the different nights. At the higher airmass values, the range in airmass differed from the mean by about ±0.1 during the observations, and less at smaller airmass.

We used the UVES-pipeline software for the reduction of the spectra. In order to maximize the S/N-ratio of the extracted spectra, all flat-fields obtained during the run were averaged. A mean ThAr-spectrum obtained during day time was used for the calibration of all spectra obtained in one night. After background subtraction and flat-fielding, the spectra were extracted as 2D-spectra using a long extraction slit covering all slices. All spectral orders of these spectra were then merged in one 2D-spectrum, keeping the information along the slit. Finally, the spectra were collapsed to a 1D-spectrum by averaging along the slit and thereby averaging the flux from all slices. The region around the CH$^+\lambda$3957 Å-line was influenced by a detector blemish. This defect only covered two CCD lines along the slit. In order to remove this defect, we also extracted spectra excluding the two affected CCD lines. The observations of of each target were then averaged to a mean spectrum. Wavelengths are reported in air and referred to the solar barycenter.

## 3. Model line profiles

We model the CH$^+$ opacity in velocity space, as in Paper I. But in this work we force the same opacity profile $\tau(v)$ on both overtones. In Paper I we preferred to fit the two overtones separately, and thus obtain independent measurements with which to assess the role of systematics. Here we incorporate the prior knowledge that both CH$^+\lambda\lambda$3957,4232 overtones share a common opacity profiles, which is true because they both stem from the same de-excited energy level (the ground state, see Casassus et al. 2005, Sect. 1)

Requiring a common velocity profile highlights the limits of our knowledge of the underlying continua on the wavelength scales of the CH$^+$ line widths. The continua can be affected by detector glitches (that is, instrumental effects that are limited to a small number of channels), or atmospheric features. In the absence of instrumental artifacts or stellar features, the two profiles

should be the same. Any difference in the fit residuals should highlight problems with the continuum definition.

In this paper we investigate how a simultaneous fit to both overtones helps constrain the CH$^+$ opacity profiles, decomposed in a set of Gaussians in velocity. This approach was attempted in Paper I to resolve cases when the $^{13}$CH$^+\lambda$4232 transition was blended with the main isotope. But in Paper I the quality of the simultaneous fits was not satisfactory. We now explain this problem in Paper I as being due to our overlooking the possibility of small shifts in the observed relative wavelengths of the two overtones, $\Delta\lambda_\circ$. Allowing for $\Delta\lambda_\circ$ produces satisfactory simultaneous fits to both overtones. Such wavelengths shifts are of the order of the uncertainties in the absolute wavelength calibration of each echelle of a few mÅ. From the fits to the 11 lines of sight acquired in 2006, we find that the maximum range of values for $\Delta\lambda_\circ$ is $3.2 \times 10^{-3}$ Å, and its $1\sigma$ scatter is $9.5 \times 10^{-4}$ Å, while the resolution element is $5.3 \times 10^{-2}$ Å.

The isotope ratio information in cases where the rare isotope is blended at $\lambda$4232 cannot be recovered without the $\lambda$3957 information. The uncertainties in the baseline definition make it impossible, using a single transition, to distinguish the rare isotope from a detector glitch. But $\lambda$4232 blends are still useful as a consistency checks. We incorporate the uncertainties in the baseline definition under $\lambda$4232 through the inclusion of extra free-parameters. The possibility of detector glitches or stellar or atmospheric features is modeled with a correction to the baseline under the interstellar absorption. We explored the possibilities of two broad types of low-level baseline corrections: 1- additive corrections, as in low-level atmospheric, stellar or CH$^+$ features, and 2- multiplicative corrections, as in flat fielding features. The low-level baselines were modeled using either an expansion in Legendre polynomials or as segmented lines. But the Legendre expansion required high orders, and thus many free-parameters, because of the condition of fixed endpoints imposed by continuity with the baseline neighboring the interstellar absorption. We obtained best results with an additive baseline correction, composed of a segmented line defined by the amplitude of spikes distributed uniformly in wavelengths.

We caution that the present technique used to measure the CH$^+$ isotopic ratio suffers from the same uncertainties inherent to any observation of absorption lines. The inferred equivalent widths depend on the exact placement of the continuum level. The uncertain definition of the baseline is a source of systematic uncertainty. However we take a conservative value for the thermal noise, with the hope of accounting for at least small variations in the baseline definition. Our noise estimate corresponds to the standard deviation of the residuals in the whole 1.5 Å windows around CH$^+\lambda\lambda$3957, 4232, after baseline and profile fitting, including detector glitches and any telluric features. Provided the baselines are realistic enough, our procedure should indeed allow for small variations among plausible baselines.

The model we use to define the underlying continua and to parameterize $\tau(v)$ is otherwise the same as in Paper I. For clarity we now itemize our new procedure:

1. extract a 1.5 Å spectrum $F(\lambda)$ centered on the CH$^+$ line, and fit a baseline with a 4−7th order Legendre polynomial; include weights to improve the quality of the baselines near the features of interest; store the RMS dispersion of the residuals as the spectrum's noise, $\sigma_F$;
2. define a model spectrum with

$$F_m(\lambda) = F_{c_1}(\lambda) \exp(-\tau(\lambda)), \qquad (1)$$

**Table 2.** Summary of the results of the fits. $f$ is given in units of $10^{-4}$. $n_{\mathrm{g}}$ is the number of Gaussian components and $W_\lambda$(4232 Å) and $W_\lambda$(3957 Å) are the equivalent widths of the respective $^{12}$CH$^+$ lines, obtained by integrating the fit solutions. Numbers in parentheses are uncertainties in the last digit. The corresponding values for the $^{13}$CH$^+$ components can be obtained by multiplying the values for the $^{12}$CH$^+$ component with $f$.

| Target | $R \pm \sigma(R)$ | $f \pm \sigma(f)$ | $n_{\mathrm{g}}$ | $W_\lambda$(4232 Å) [mÅ] | $W_\lambda$(3957 Å) [mÅ] |
|---|---|---|---|---|---|
| HD 23480 | 96.5±16.3 | 103.6±17.5 | 1 | 14.94 (2) | 8.82 (3) |
| HD 35149 | 49.4± 8.2 | 202.2±33.5 | 2 | 9.48 (3) | 5.29 (3) |
| HD 37903 | 97.5±27.2 | 102.5±28.6 | 2 | 10.05 (3) | 5.80 (4) |
| HD 52382 | 59.7±13.5 | 167.6±37.8 | 2 | 19.20 (3) | 11.01 (4) |
| HD 53974 | 91.5±18.8 | 109.2±22.5 | 2 | 11.76 (2) | 6.68 (3) |
| HD 58510 | 43.7±10.8 | 228.9±56.5 | 3 | 10.30 (3) | 5.75 (4) |
| HD 73882 | 79.7±14.5 | 125.5±22.9 | 2 | 17.45 (3) | 9.86 (4) |
| HD 75149 | 102.7±21.0 | 97.3±19.9 | 2 | 10.22 (2) | 5.73 (3) |
| HD 76341 | 56.2± 8.1 | 177.8±25.6 | 2 | 38.43 (3) | 23.10 (4) |
| HD 91452 | 76.0±23.3 | 131.5±40.2 | 2 | 8.75 (3) | 4.86 (4) |
| HD 92964 | 146.7±39.3 | 68.2±18.3 | 2 | 8.06 (2) | 4.46 (2) |
| $\zeta$ Oph | 80.9± 3.0 | 123.5± 4.5 | 2 | 23.42 (1) | 13.82 (1) |
| HD 110432 | 69.1± 4.4 | 144.8± 9.2 | 2 | 13.74 (2) | 7.88 (2) |
| HD 152235 | 92.2± 4.9 | 108.5± 5.7 | 3 | 41.78 (3) | 24.88 (2) |

where the line absorption opacity $\tau$ is a superposition of $n_{\mathrm{g}} = 1$ to 4 Gaussians common to each isotope, with $^{13}$CH$^+$ components sharing the parameters of the $^{12}$CH$^+$ components, except that their centroids are translated by a velocity shift $\Delta v_{\mathrm{iso}}$, and their amplitude are scaled by a factor $f = {}^{13}$CH$^+/^{12}$CH$^+$, kept as a free parameter:

$$\tau(\lambda) = \sum_{i=1}^{n_{\mathrm{g}}} \tau_i^\circ \exp\left(-0.5(\lambda - \lambda_i^\circ)^2/\sigma_i^{\circ 2}\right)$$
$$+ \sum_{i=1}^{n_{\mathrm{g}}} f\,\tau_i^\circ \exp\left(-0.5(\lambda - \lambda_i^\circ(1 + \Delta v_{\mathrm{iso}}/c))^2/\sigma_i^{\circ 2}\right); \quad (2)$$

3. the wavelength shift between each isotope is taken as a free parameter, allowed to vary over a resolution element;
4. in cases of blends or suspected glitches we include an additive correction to the baseline (details are given in the description of results from individual lines of sights). The corrections applied to the continuum level derived from Step 1, are parameterized using a segmented line defined by $n_{\mathrm{spikes}}$ points distributed in equal wavelength intervals under the whole CH$^+$ profile;
5. since blends always occur under $\lambda$4232, we artificially increased the noise under the fundamental tone by a factor of 10, thereby allowing the otherwise noisier overtone to have a stronger influence in the optimization;
6. optimize the model parameters by minimizing $\chi^2 = \sum_j (F(\lambda_j) - F_{\mathrm{m}}(\lambda_j))^2/\sigma_{\mathrm{F}}^2$, using the noise from Step 1. The optimization was carried with the PDL::Minuit package (based on the Minuit optimization library from CERN);
7. update the noise of the stellar spectrum by replacing $\sigma_{\mathrm{F}}$ with the root mean square (RMS) dispersion of the residuals (the difference between the observed and model spectra over the whole 1.5 Å window);
8. estimate the uncertainty in model parameters by two methods:
   (a) search parameter space for the $\Delta \chi^2 = 1$ contour defining the region enclosing 68.3% confidence level.
   (b) estimate $1\sigma$ uncertainties from the curvature matrix of $\chi^2$ (i.e. approximate to normal errors).
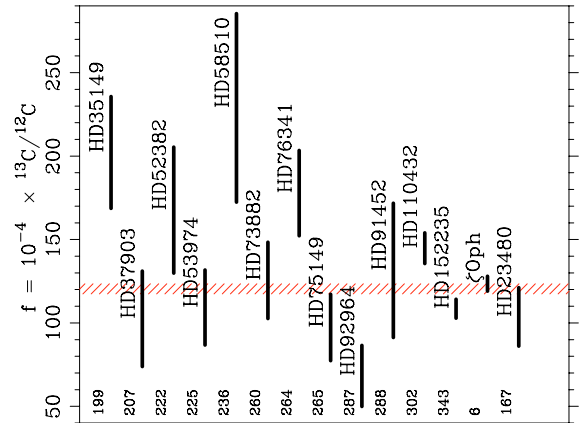


**Fig. 1.** A plot of individual $f$ values for the lines of sight studied in this work. The galactic longitude of the targets is also indicated. The thick lines are $\pm 1\sigma$ uncertainties ($2\sigma$ in total length). The hatched box is the weighted average of the measurements in the figure, and should be representative of the local ISM. The height of the hatched rectangle is $\pm 1\sigma$. This value is $\langle f \rangle = (120.46 \pm 3.02) \times 10^{-4}$. The corresponding average for $R$ values is $\langle R \rangle = 76.27 \pm 1.94$.

## 4. Results of the fits

### 4.1. Average properties of the dataset

In the following we discuss the results of our fits for all lines of sight. In order to increase the number of lines of sight, we include, in addition to the targets observed in Jan. 2006 also the best targets from Paper I: $\zeta$ Oph, HD 110432 and HD 152235. These stars have been observed with the same instrument setting but were analyzed differently. In order not to introduce any bias in our results, we applied the fitting method described above also for these stars. The results for $R$ and $f$ differ only slightly from the results in Paper I. These results are consistent to within the errors.

The results for the fits of all targets are given in Table 2 and are plotted in Fig. 1.

In Paper I we summarized our measurements in terms of $R = {}^{12}$C/$^{13}$C. But it is preferable to use $f = 1/R$ since for $f$ the noisiest factor occurs in the numerator. We combine all $f$ measurements in a weighted average $\langle f \rangle$ by weighting each line of
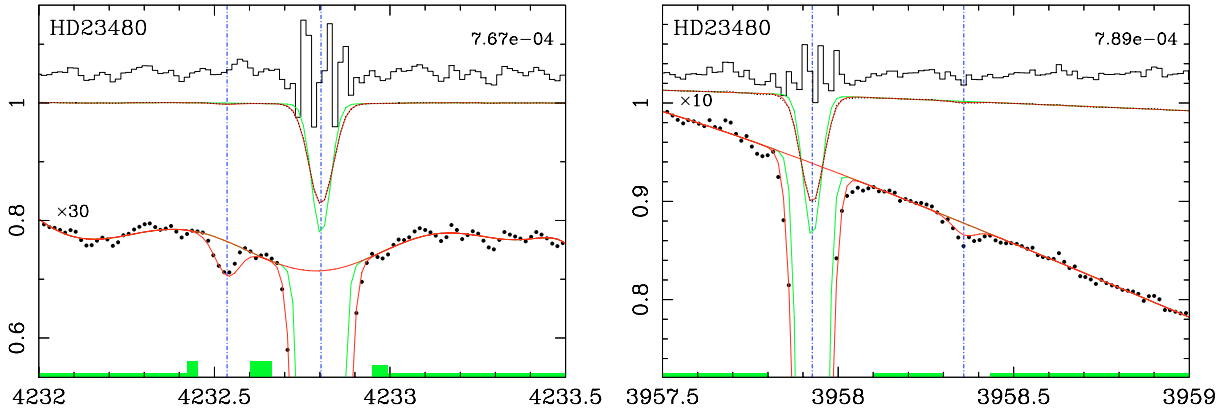
**Fig. 2.** Spectra of HD 23480. Wavelengths are in Å, and flux densities in arbitrary units. The individual Gaussian components comprising the fit, prior to folding with the instrumental response, are shown only on $^{12}$CH$^+$ as light gray lines, but are omitted from $^{13}$CH$^+$ for clarity. The vertical dashed lines mark the line centroids, at the average of the Gaussian centroids weighted by their equivalent widths. The units of the $y$-axis are arbitrary, and are scaled so that the median of the object spectrum is unity. Also shown is a magnified version of the object spectrum, by the factor indicated on the figure, and offset for clarity. The residual spectrum is shown on top of the object spectrum, and is also magnified by the factor indicated on the figure. The noise used to compute the significance of the fits is shown at the top right. The noise is the RMS dispersion of the residual spectrum, and is in the same units as the $y$-axis. The height of the shaded rectangles on top of the $x$-axis indicates the relative weights used in the baseline definition.

sight by $1/\sigma^2$, where $\sigma$ is the root-mean-square uncertainty on $f$. We find $\langle f \rangle = (120.46 \pm 3.02) \times 10^{-4}$. The weighted scatter of $f$ values is $6.3 \times \sigma(\langle f \rangle)$. This shows that the scatter is caused by statistically different isotope ratios. That is, the scatter is intrinsic and not merely a result of statistical fluctuations about a *single* mean value. Indeed, applying the $\chi^2$ test for the null hypothesis that all measurements derive from a single value, we find that the reduced $\chi^2$ is 3.02 for 14 data points and 1 free parameter (i.e. $\langle f \rangle$). Such a $\chi^2$ value allows us to state that the observed distribution of $f$ values has a significant scatter with essentially 100% confidence. In other words, there is no single isotope ratio for this set of sources.

The corresponding average for $R$ values is $\langle R \rangle = 76.27 \pm 1.94$. This is to be compared with the value of $R = 78.27 \pm 1.84$ published in Casassus et al. (2005). The previous average ratio was calculated from a smaller sample.

In contrast to $f$, the isotope ratio $R = 1/f$ is not normally distributed, so that the uncertainties on $R$ are not directly related to confidence levels. Therefore the ISM statistics over the sample of sight-lines must be determined from $f$. Unfortunately in Paper I we extracted statistics on $R$ values, rather than $f$ values. Here we present an improved approach. The conclusions from Paper I still hold, however. The positive skew in $R$ becomes negligible for smaller uncertainties and larger $R$. In the Paper I data, the ISM scatter in $R$ is 7% smaller than that in $f$, relative to the uncertainties on their weighted average. The variations in $f$ towards HD 110432 and HD 152235 are 3.4$\sigma$ (rather than 4.3$\sigma$ in $R$), and are 3.5$\sigma$ towards HD 110432 and HD 170740 (rather than 3.2$\sigma$).

### 4.2. Notes on individual objects

#### 4.2.1. HD 23480

HD 23480 (=23 Tau = Merope) is a well-known member of the Pleiades cluster and the only target in our list which has a published $^{12}$C/$^{13}$C-ratio (41±9, Hawkins & Jura 1987). We observed it, despite its northern location, as a reference target. Because of its position the sky, the airmass during our observations was relatively high. Our result is in disagreement with Hawkins & Jura (41 ± 9, 1987): we do not confirm their low value of $R$ toward

HD 23480. The UVES CH$^+$ spectrum (see Fig. 2) appears to be free of blends or artifacts.

#### 4.2.2. HD 35149

A detailed study of the interstellar medium towards HD 35149 (=23 Ori) based on high resolution UV spectra has been published by Welty et al. (1999). Ádámkovics et al. (2003) searched the star for rotationally resolved C$_3$, but did not detect this molecule towards HD 35149. Measurements of diffuse interstellar bands towards the star have been published by Thorburn et al. (2003). The UVES CH$^+$ spectrum (see Fig. 3) appears to be free of blends or artifacts.

#### 4.2.3. HD 37903

HD 37903 is the illuminating star of the reflection nebula NGC 2023. A detailed study of the interstellar medium towards HD 37903, based on ORFEUS UV data, has been published by Lee et al. (2002). This star has previously been observed in the CH$^+$-line by Gredel et al. (1993). The UVES CH$^+$ spectrum (see Fig. 4) appears to be free of blends or artifacts.

#### 4.2.4. HD 52266

HD 52266 is considered a field star, but is projected close to CMa OB1. de Wit et al. (2004) found evidence for a cluster near the star. No detailed study of the interstellar medium in this direction has been published so far.

This spectrum is very shallow because we quickly ended the observations with Kueyen when we found that the line of sight to HD 52266 is very structured, and thus useless for the determination of an isotope ratio. The multiple velocity components are nonetheless faint enough to have escaped detection in our FEROS preselection. The UVES CH$^+$ spectrum is shown in Fig. 5.
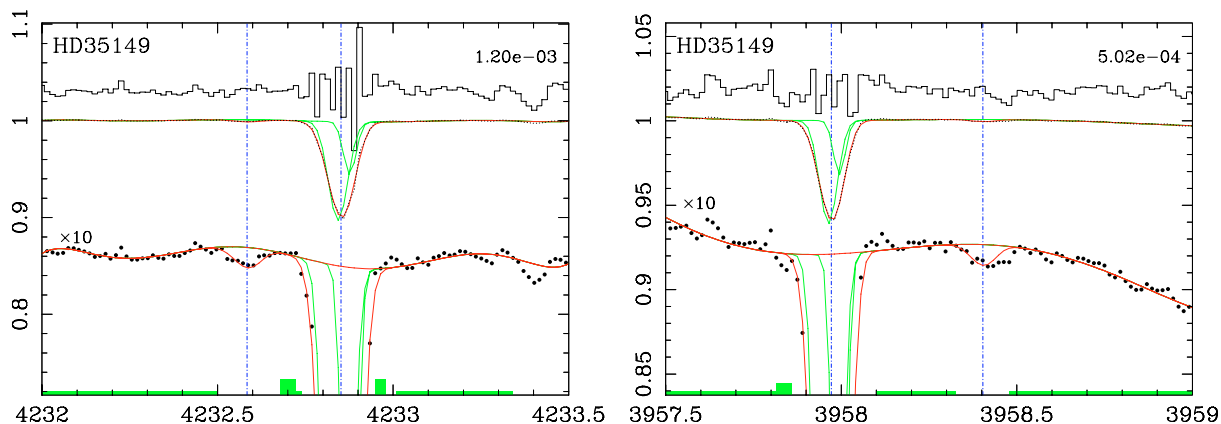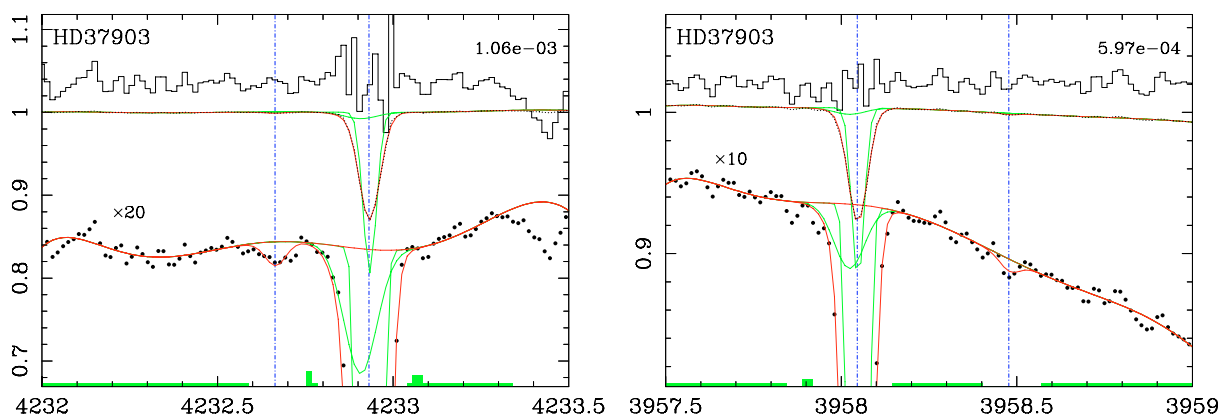
**Fig. 3.** Same as Fig. 2, but for HD 35149.



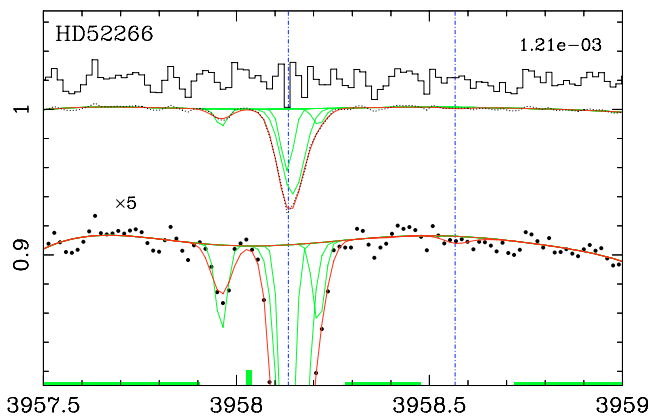**Fig. 4.** Same as Fig. 2, but for HD 37903.



**Fig. 5.** Same as Fig. 2, but for HD 52266.

### 4.2.5. HD 52382

This star is a member of the CMa OB1 association and has previously been observed in the CH$^+$-line by Gredel (1997). The UVES CH$^+$ spectrum (see Fig. 6) appears to be free of blends or artifacts.

### 4.2.6. HD 53974

This star is considered a field Be star by Zorec et al. (2005). No detailed study of the interstellar medium in this direction has been published so far. The UVES CH$^+$ spectrum (see Fig. 7) appears to be free of blends or artifacts.

### 4.2.7. HD 58510

HD 58510 is a little-studied B1ab supergiant. No detailed study of the interstellar medium in this direction has been published so far.

Although the fundamental $^{13}$CH$^+$ tone is only marginally blended, the baseline at $\lambda$4232 shows a break right under $^{13}$CH$^+$, which is very difficult to account for. The UVES CH$^+$ spectrum is shown in Fig. 8.

### 4.2.8. HD 73882

This member of Vela OB1 has previously been observed in the CH$^+$-line by Gredel et al. (1993). The star is located in the Gum
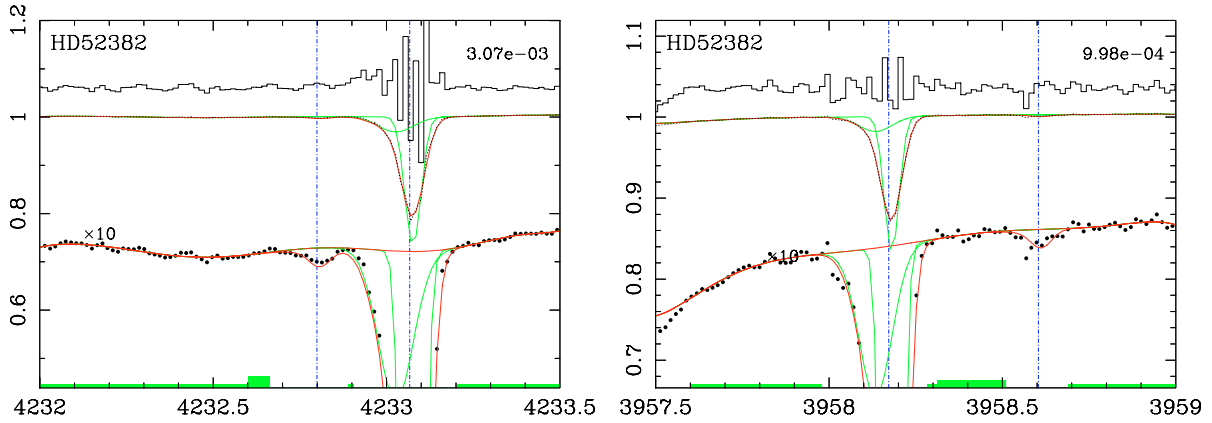
**Fig. 6.** Same as Fig. 2, but for HD 52382.
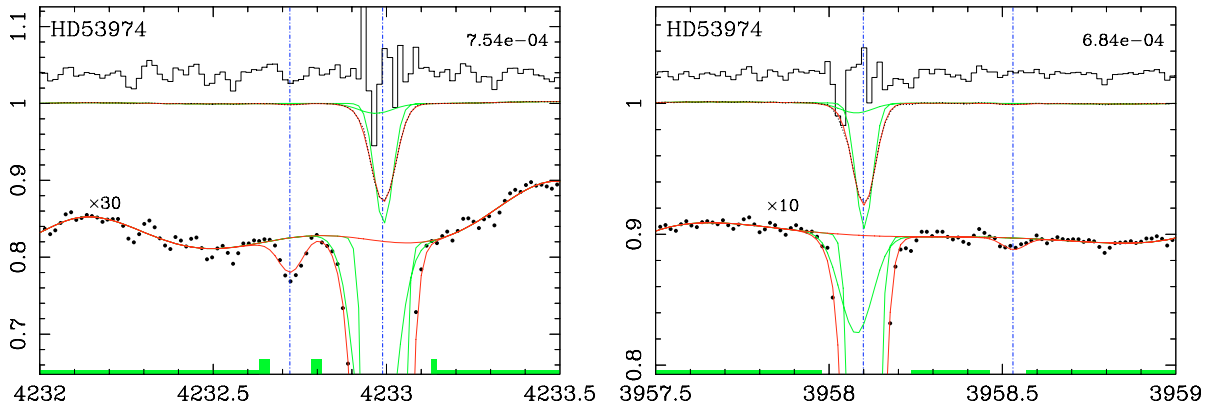


**Fig. 7.** Same as Fig. 2, but for HD 53974.
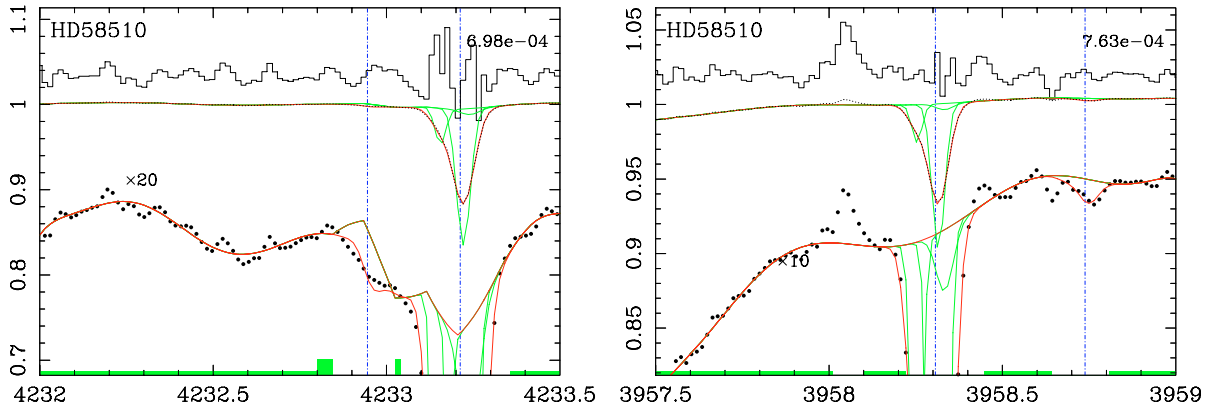


**Fig. 8.** Same as Fig. 2, but for HD 58510.

nebula. HD 73882 has been observed in the far ultraviolet with FUSE. These observations have been used to study e.g. the interstellar deuterium abundance (Ferlet et al. 2000) and the interstellar extinction towards HD 73882 (Sofia et al. 2005). FUSE spectra of the star have also been published by Snow et al. (2002) and Rachford et al. (2002). IUE and FUSE data have been used by Sonnentrucker et al. (2007) to determine a $^{12}$CO/$^{13}$CO column density ratio of 25 towards HD 73882, significantly below our value for $^{12}$C/$^{13}$C. Since Sonnentrucker et al. (2007) find particularly low $^{12}$CO/$^{13}$CO-ratios in lines of sight which sample cool and dense gas, they interpret this finding as evidence for chemical fractionation of CO in cool and dense regions. The UVES CH$^+$ spectrum (see Fig. 9) appears to be free of blends or artifacts.

### 4.2.9. HD 75149

This star is a member of the Vela OB1 association and has previously been observed in the CH$^+$-line by Gredel (1997). Gredel et al. (2002) and Gredel (1999) also observed the star in the interstellar CN and C$_2$ lines, respectively. Observations of interstellar Na I and Ca II have been published by Cha & Sembach (2000). The UVES CH$^+$ spectrum (see Fig. 10) appears to be free of blends or artifacts.

### 4.2.10. HD 76341

Although this star is not in the list of Humphreys (1978), it is considered by Reed (2000) as a probable member of the
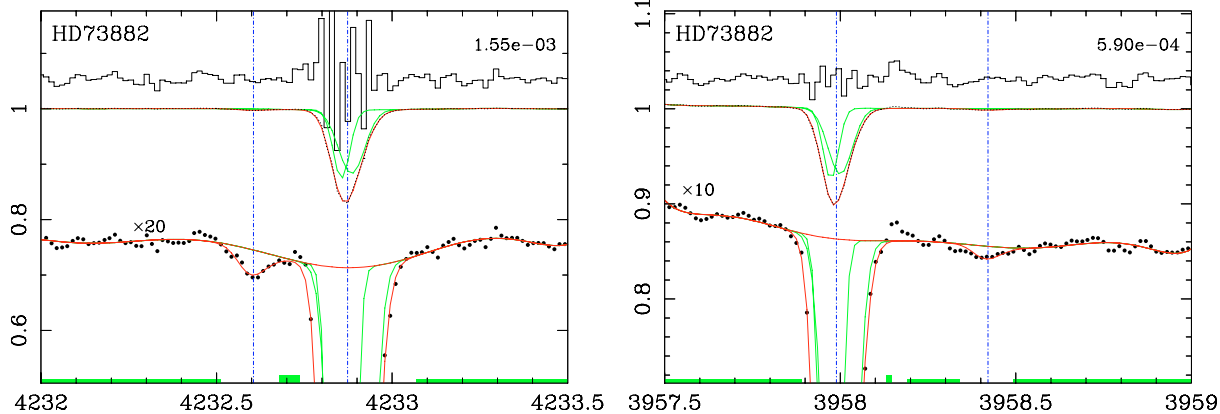
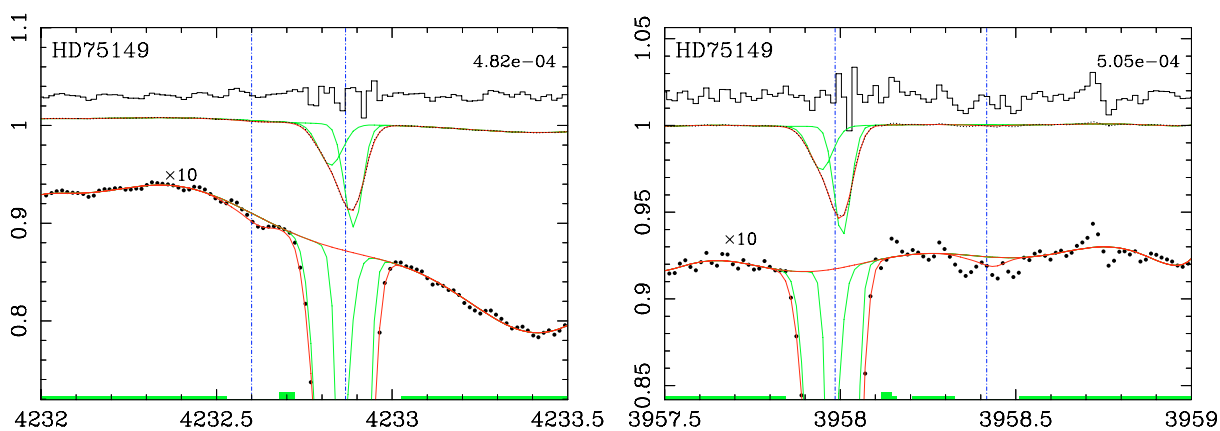**Fig. 9.** Same as Fig. 2, but for HD 73882.



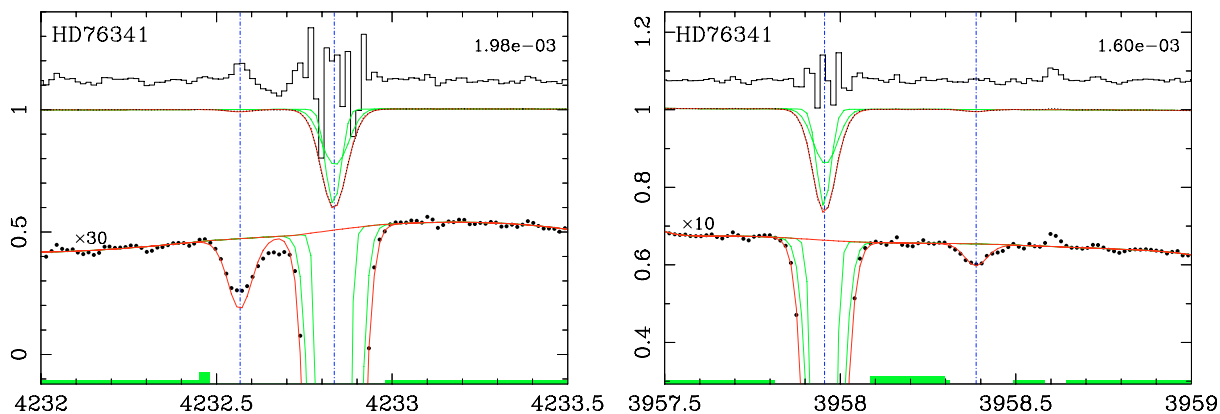**Fig. 10.** Same as Fig. 2, but for HD 75149.



**Fig. 11.** Same as Fig. 2, but for HD 76341.

OB association Vela OB1. Nichols & Slavin (2004) searched for unusually strong excited interstellar C I in stars seen through the Vela supernova remnant, indicating shock excitation, and found several stars with unusually strong C I. Both HD 35149 and HD 76341 are included in their sample, but do not show unusually strong C I.

Although relatively faint, HD 76341 gives us the best measurement of $^{12}$CH$^+$/$^{13}$CH$^+$. It has a very sharp and relatively strong CH$^+$-line.

The fundamental $^{13}$CH$^+$ absorption at $\lambda$4232 appears to be blended with the main isotope, as well as affected by baseline

uncertainties (atmospheric, and instrumental detector glitches). By artificially changing the noise under $\lambda$3957 and $\lambda$4232, we can test the effect of imposing the $R$ value from each overtone. We find it is impossible to fit the $^{13}$CH$^+$$\lambda$4232 simultaneously with $^{12}$CH$^+$$\lambda$4232 without changing the baseline under $^{13}$CH$^+$$\lambda$4232 by deviations from the Legendre polynomial fit (step 1) comparable to the $^{13}$CH$^+$ line depth. On the other hand, if we artificially decrease the noise under the overtone $^{13}$CH$^+$ absorption at $\lambda$3957, then it is possible to also fit $^{12}$CH$^+$ in both overtones. Figrue 11 shows the result of imposing the $^{13}$CH$^+$$\lambda$3957 profile. It is clear that the observed spectral points
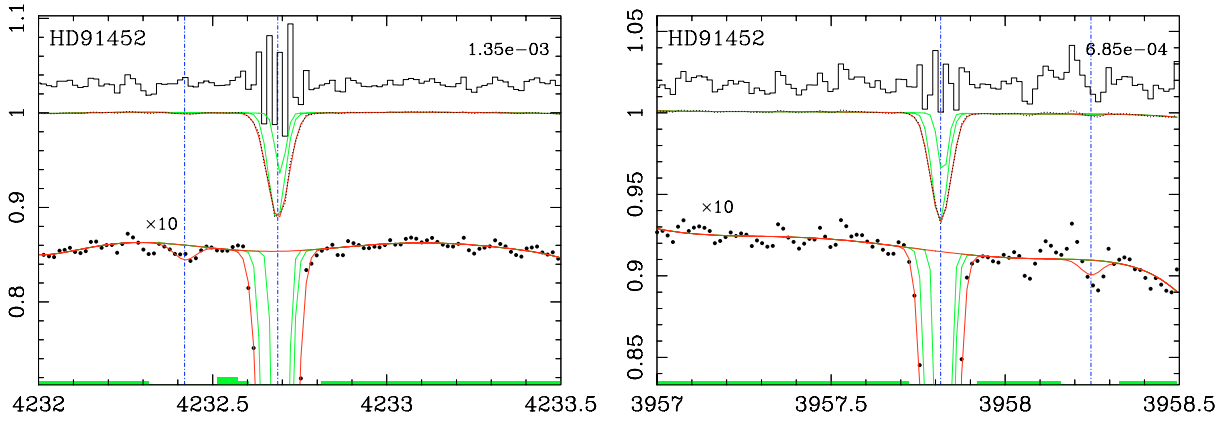
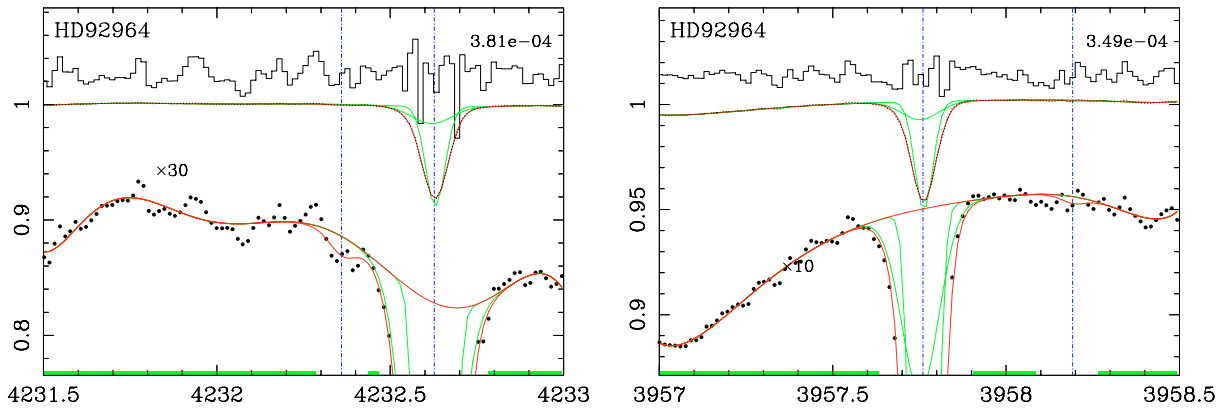**Fig. 12.** Same as Fig. 2, but for HD 91452.



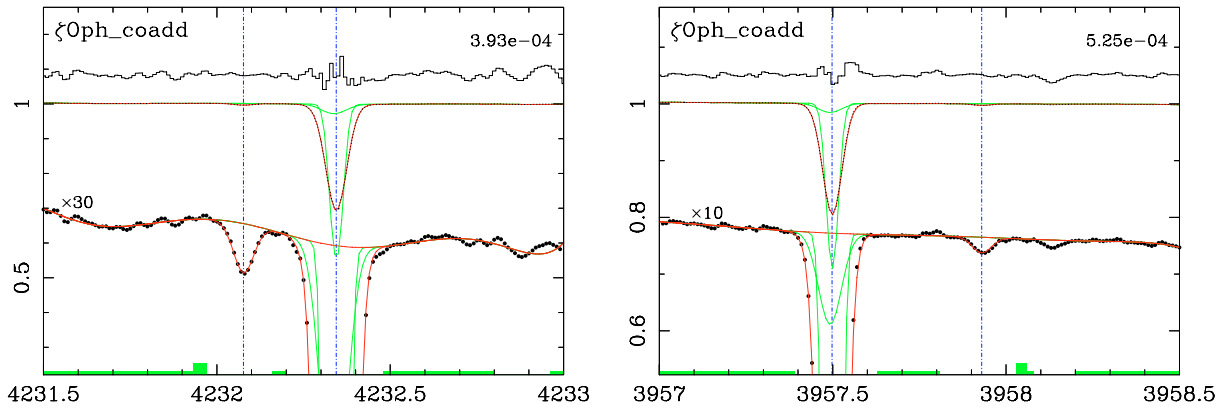**Fig. 13.** Same as Fig. 2, but for HD 92964.



**Fig. 14.** Same as Fig. 2, but for ζ Oph.

in $^{13}$CH$^+$ $\lambda$4232 do not share the same profile as the other 3 lines, $^{13}$CH$^+$ $\lambda$4232 is therefore affected by either atmospheric features or detector glitches, of the type seen at $\lambda = 3858.6$ Å. The uncertainties on $R$ are those obtained by varying only $R$ and keeping fixed all other parameters. The UVES CH$^+$ spectrum is shown in Fig. 11.

### 4.2.11. HD 91452

de Wit et al. (2004) unsuccessfully searched for a cluster near HD 91452. According to de Wit et al. (2005), HD 91452 is a runaway O-type star. No detailed study of the interstellar medium in this direction has been published so far. The UVES CH$^+$ spectrum (see Fig. 12) appears to be free of blends or artifacts.

### 4.2.12. HD 92964

This star is a member of the OB association Car OB1. No detailed study of the interstellar medium in this direction has been published so far. The UVES CH$^+$ spectrum (see Fig. 13) appears to be free of detectable blends or artifacts.

### 4.2.13. ζ Oph

Because of its brightness and it has narrow, rather simple interstellar line profiles, ζ Oph is a prototype star for studies of the interstellar medium, also for the C$^{12}$/C$^{13}$ ratio. The UVES CH$^+$ spectrum is shown in Fig. 14. For a more detailed discussion see Paper I.

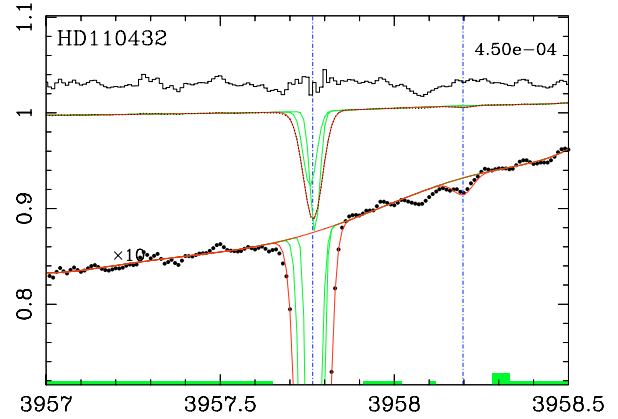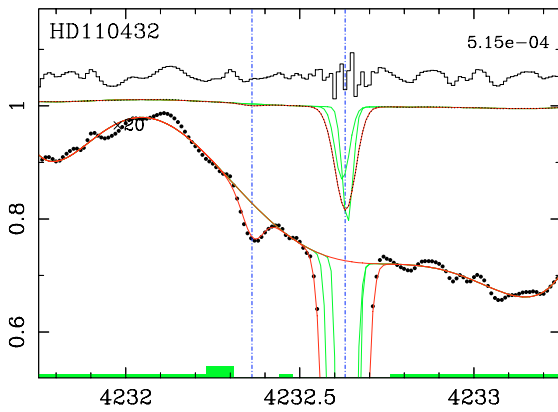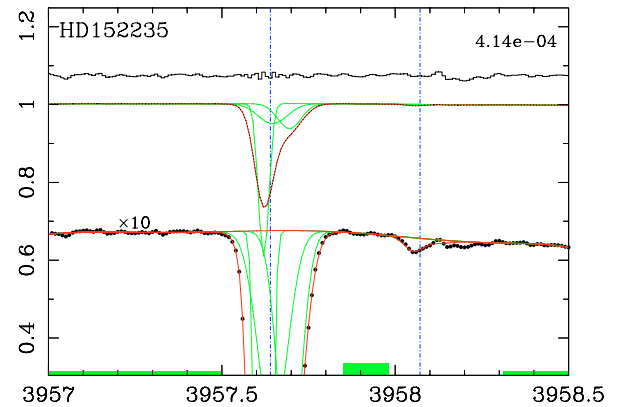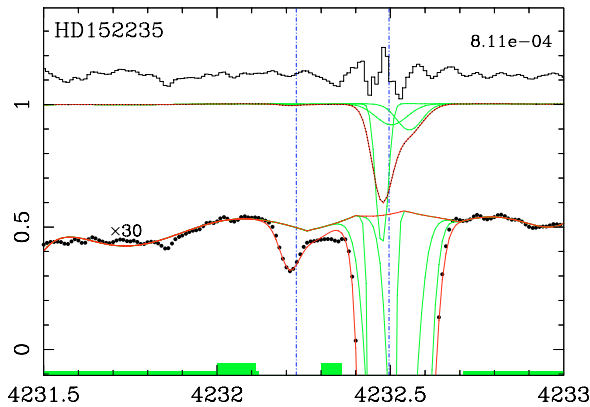**Fig. 15.** Same as Fig. 2, but for HD 110432.



**Fig. 16.** Same as Fig. 2, but for HD 152235.

### 4.2.14. HD 110432

This star was also discussed in Paper I. The sight-line to HD 110432 is one of the cleanest lines of sight studied in Paper I. The UVES CH$^+$ spectrum is shown in Fig. 15.

### 4.2.15. HD 152235

This star is another star from Paper I. We treated this case as a blend, since the $^{13}$CH$^+$ profile just overlaps with $^{12}$CH$^+$ in the fundamental tone. We exaggerated the noise for $\lambda 4232$ by a factor of 3, instead of 10 as in the other blended cases. There is possible telluric absorption to the red side of $^{13}$CH$^+\lambda 3957$. The UVES CH$^+$ spectrum is shown Fig. 16.

## 5. Discussion and conclusions

Our systematic search for stars with clean line profiles in CH$^+$ and large equivalent widths, which are suitable for isotope studies, has resulted in a much larger sample of reliable $^{12}$C/$^{13}$C isotope ratios from optical observations.

The VLT-UVES spectra of CH$^+$ absorption in the lines of sight towards 14 stars have allowed us to measure the carbon isotopic ratio $R = {}^{12}$C/$^{13}$C with unprecedented accuracy. This significant extension of the sample of Casassus et al. (2005) allows us to strengthen their conclusion that there is truly a significant scatter in the local ISM. Averaging our measurements for the 14 lines of sight gives a value representative of the local ISM: $\langle R \rangle = 76.27 \pm 1.94$. This mean ratio is in excellent agreement with the local ratio determined from radio astronomical measurements of CO and H$_2$CO (76 ± 7, Wilson & Rood 1994),

and also in good agreement with more recent determinations from CN ($\approx$68, Milam et al. 2005). This agreement obtained from different molecule probes suggests that chemical fractionation and selective dissociation do *not* play a major role for the CO, H$_2$CO and CN molecules. The results of Sonnentrucker et al. (2007) suggest, however, that CO may be somewhat affected by chemical fractionation in cool and dense regions.

The weighted scatter of $f$ values is $6.3 \times \sigma(\langle f \rangle)$. This shows directly that the $^{12}$C/$^{13}$C isotope ratios vary on the relatively small spatial scales which we sample. Considering this intrinsic scatter of the $^{12}$C/$^{13}$C ratio in the ISM, the solar carbon isotope ratio of 89 is indistinguishable from the present-day value, even after 4.5 Gyr of galactic evolution. This statement is not affected by instrumental uncertainties, although a sampling bias could distort our ISM value. Of course, this conclusion is based on the assumption that the solar system ratio is representative for the galactocentric distance $R_\odot = 8.5$ kpc, 4.5 Gyr ago. Since we have shown that the interstellar $^{12}$C/$^{13}$C isotope ratio is spatially variable now, it is not clear whether the solar value of $^{12}$C/$^{13}$C = 89 was characteristic for the local ratio, 4.5 Gyr ago. However, there is also no strong evidence that the solar value is atypical: Although it has been claimed that the sun is overabundant in metals, especially in carbon and oxygen, compared to the local ISM, the solar carbon and oxygen abundances have been revised downwards. Recent papers (e.g. Allende Prieto 2007) find good agreement for the carbon and oxygen abundance in the sun, the local ISM and young stars. Comets show a $^{12}$C/$^{13}$C ratio consistent with the photospheric solar value (e.g. Manfroid et al. 2005). Therefore it also seems unlikely that the interstellar $^{12}$C/$^{13}$C ratio was modified 4.5 Gyr ago from the value in the

solar nebula by fractionation of carbon isotopes during the formation of the sun.

Therefore we conclude that there is no evidence that the solar $^{12}$C/$^{13}$C ratio is atypical for the solar neighborhood 4.5 Gyr ago. It is plausible however, that the average value for the solar neighborhood was somewhat different from the solar value, possibly by an amount similar to the present day variations. A small decrease of the average $^{12}$C/$^{13}$C ratio in the solar neighborhood during the lifetime of the solar nebula is therefore certainly possible.

The $^{12}$C/$^{13}$C ratio increases with galactocentric distance (Wilson & Rood 1994), by about 7.5 ± 1.9 per kpc. Therefore, a comparison of the present-day local $^{12}$C/$^{13}$C ratio with the solar photospheric value should also take into account that the sun was born at a different galactocentric distance (Wielen & Wilson 1997). According to Wielen et al. (1996), the sun may have migrated from its birth-place in the inner part of the Galaxy outward to its present galactocentric location by 1.9 ± 0.9 kpc during its lifetime. This effect would require significant changes in the $^{12}$C/$^{13}$C ratio.

Early models for the $^{12}$C/$^{13}$C isotope ratio were able to model the significant decrease of the local ratio over the lifetime of the sun (about a factor two), which were assumed to be present at that time. However, the models require some fine tuning and calibration, so that a smaller decrease is not in obvious conflict with the models. Nevertheless, some variation of the $^{12}$C/$^{13}$C isotope ratio is to be expected. New models of the chemical evolution of the Galaxy are required to take into account the new observational results.

A larger sample of stars will allow a better estimate of the average ISM value. In addition, these observations will allow to determine the scale of the variations of the isotope ratio and thus the efficiency of mixing on different scales.

## References

Ádámkovics, M., Blake, G. A., & McCall, B. J. 2003, ApJ, 595, 235
Allende Prieto, M. 2007, in 14th Cambridge Workshop on Cool Stars, Stellar Systems, and the Sun, ed. G. van Belle [arXiv:astro-ph/0702429v1]
Anders, E., & Grevesse, N. 1989, Geochim. Cosmochim. Acta, 53, 197
Casassus, S., Stahl, O., & Wilson, T. L. 2005, A&A, 441, 181
Cha, A. N., & Sembach, K. R. 2000, ApJS, 126, 399
de Wit, W. J., Testi, L., Palla, F., Vanzi, L., & Zinnecker, H. 2004, A&A, 425, 937
de Wit, W. J., Testi, L., Palla, F., & Zinnecker, H. 2005, A&A, 437, 247
Ferlet, R., André, M., Hébrard, G., et al. 2000, ApJ, 538, L69
Gredel, R. 1997, A&A, 320, 929
Gredel, R. 1999, A&A, 351, 657
Gredel, R., van Dishoeck, E. F., & Black, J. H. 1993, A&A, 269, 477
Gredel, R., Pineau des Forêts, G., & Federman, S. R. 2002, A&A, 389, 993
Hawkins, I., & Jura, M. 1987, ApJ, 317, 926
Humphreys, R. M. 1978, ApJS, 38, 309
Lee, D.-H., Min, K.-W., Federman, S. R., et al. 2002, ApJ, 575, 234
Maíz-Apellániz, J., Walborn, N. R., Galué, H. Á., & Wei, L. H. 2004, ApJS, 151, 103
Manfroid, J., Jehin, E., Hutsemékers, D., et al. 2005, A&A, 432, L5
Milam, S. N., Savage, C., Brewster, M. A., Ziurys, L. M., & Wyckoff, S. 2005, ApJ, 634, 1126
Nichols, J. S., & Slavin, J. D. 2004, ApJ, 610, 285
Prantzos, N. 2001, in Cosmic evolution, ed. E. Vangioni-Flam, R. Ferlet, & M. Lemoine, 233
Prantzos, N., Aubert, O., & Audouze, J. 1996, A&A, 309, 760
Rachford, B. L., Snow, T. P., Tumlinson, J., et al. 2002, ApJ, 577, 221
Reed, B. C. 2000, AJ, 119, 1855
Savage, C., Apponi, A. J., Ziurys, L. M., & Wyckoff, S. 2002, ApJ, 578, 211
Snow, T. P., Rachford, B. L., & Figoski, L. 2002, ApJ, 573, 662
Sofia, U. J., Wolff, M. J., Rachford, B., et al. 2005, ApJ, 625, 167
Sonnentrucker, P., Welty, D. E., Thorburn, J. A., & York, D. G. 2007, ApJS, 168, 58
Stahl, O., & Wilson, T. L. 1992, A&A, 254, 327
Thorburn, J. A., Hobbs, L. M., McCall, B. J., et al. 2003, ApJ, 584, 339
Tosi, M. 2000, in The Evolution of the Milky Way: Stars versus Clusters, ed. F. Matteucci, & F. Giovannelli, 505
Watson, W. D., Anicich, V. G., & Huntress, W. T. 1976, ApJ, 205, L165
Welty, D. E., Hobbs, L. M., Lauroesch, J. T., et al. 1999, ApJS, 124, 465
Wielen, R., & Wilson, T. L. 1997, A&A, 326, 139
Wielen, R., Fuchs, B., & Dettbarn, C. 1996, A&A, 314, 438
Wilson, T. L., & Rood, R. 1994, ARA&A, 32, 191
Zorec, J., Frémat, Y., & Cidale, L. 2005, A&A, 441, 235